Capture reactions into Borromean two-proton systems at *rp* waiting points

D. Hove, A. S. Jensen, H. O. U. Fynbo, N. T. Zinner, and D. V. Fedorov
Department of Physics and Astronomy, Aarhus University, DK-8000 Aarhus C, Denmark

E. Garrido
Instituto de Estructura de la Materia, IEM-CSIC, Serrano 123, E-28006 Madrid, Spain
(Received 8 September 2015; revised manuscript received 2 November 2015; published 1 February 2016)

We investigate even-even two-proton Borromean systems at prominent intermediate heavy waiting points for the rapid proton capture process. The most likely single-particle levels are used to calculate three-body energy and structure as a function of proton-core resonance energy. We establish a linear dependence between two- and three-body energies with the same slope, but the absolute value slightly dependent on partial wave structure. Using these relations we estimate low-lying excited states in the isotones following the critical waiting points. The capture rate for producing a Borromean bound state is described based on a full three-body calculation for temperatures about 0.1–10 GK. In addition, a simple rate expression, depending only on a single resonance state, is found to comply with the three-body calculation for temperatures between 0.1 and 4 GK. The rate calculations are valid for both direct and sequential capture paths. As a result the relevant path of the radiative capture reactions can be determined. We present results for $E1$ and $E2$ photon emission, and discuss occurrence preferences in general as well as relative sizes of these most likely processes. Finally, we present a method for estimating proton capture rates in the region around the critical waiting points.

DOI: 10.1103/PhysRevC.93.024601

I. INTRODUCTION

A number of proton dripline nuclei are of particular interest as waiting points in the rapid-proton capture (rp) process expected to be active in the accretion of a close binary system containing a neutron star and resulting in an x-ray burst [1–5]. When the proton binding energy becomes negative at the dripline another proton is needed to produce the Borromean system (a bound system with unbound subsystems). The effective lifetime of the critical waiting points in a stellar environment is a central quantity in the understanding of this astrophysical process. This depends crucially on both proton binding of the waiting point plus one and two protons, as well as the reaction rate forming these nuclei [6,7]. The current estimates still result in an uncertainty in the effective lifetime of several orders of magnitude [8,9]. The energy, capture time, and capture mechanism can be explored through three-body calculations. Relatively few full three-body results have been published, although many capture rates have been estimated using various approximations [6,7,10]. So far the three-body results have been limited to nuclei lighter than ^{38}Ca [7,10]. However, three heavier critical waiting points exist, which have as of yet not been treated from a few-body perspective. These critical waiting points are ^{64}Ge, ^{68}Se, and ^{72}Kr [2,11]. Recent efforts suggest ^{64}Ge is of less importance than previously thought, while ^{68}Se, on the other hand, is thought to be of prime importance [12,13].

Weakly bound nuclear states have been successfully described as few-body structures in a number of cases for a long time [14,15]. The most thorough and abundant theoretical investigations exist along the neutron dripline [16,17], but also excited states of ordinary nuclei have revealed this structure [14], and recently a few medium-heavy α-dripline nuclei were suggested to be of 2-α + core structure [18]. Few-body formalism is most often applied to the very light nuclei, where the constituent particles have a less intricate structure. For instance, few-body models have been applied successfully in describing the bridging of the mass gaps at $A = 5$ and 8 [19,20]. Likewise, three-body models have been applied for two-neutron plus core systems to provide astrophysically relevant production rates at the neutron dripline [17,21] again for the very light systems. The next step to the proton dripline nuclei and two-proton structure has been investigated for special, relatively light nuclei [7,10,22,23], but much less for heavier systems. For the heavier nuclei the increased Coulomb interaction severely complicates at least the numerical calculations, if not the conceptual picture.

The location of the proton dripline—which is rather irregular—is fairly well established at least up to around the medium-heavy nuclei [6,24–26], but details of the nuclear properties are often very scarce. The most important quantity is of course the binding energy and the related stability which provides the definition of the dripline. Near the neutron dripline it is established that low-angular momentum single-particle states produce spatially extended two-neutron halo nuclei [14]. This few-body picture is less effective at the proton dripline since the unavoidable Coulomb interaction would produce a confining barrier for bound nuclei. However, a cluster structure of decoupled core and proton degrees of freedom still constitutes a fair description provided the core is relatively tightly bound, and the few-body binding energy is very small or perhaps even negative.

Performing two and three-body calculations at the proton dripline requires information about the single-proton orbits, in particular their energy, as well as spin and parity relative to the core nucleus. Measured values are in most cases not available for these ground and low-lying excited states, which should be occupied by the protons just before or after reaching the dripline. Instead, trends from neighboring nuclei and

especially the results from mean-field calculations are used. The inherent uncertainties can be ascertained by variation of these input parameters.

The purpose of this paper is first of all to provide characterizing information about the rp process at waiting points for intermediate heavy nuclei along the proton dripline. The intent is to provide an initial method for approaching nuclei around the critical waiting points from a three-body perspective. The Borromean three-body structure is crucial as an intermediate structure which therefore first must be investigated. We shall determine structure and constraints for the decisive two-body proton-core energies. This is used to present a general method for estimating proton capture rates given very sparse experimental information.

In Sec. II we briefly give the theoretical framework and pertinent formulas for both the few-body formalism and the three-body reaction rates, as well as the parametric choices of the potentials. Section III contains a detailed description of the ground state properties of the Borromean proton dripline systems of interest. Both the relation between two- and three-body energies and the structure of the ground state is examined in detail. Section IV gives calculated results for the radiative capture reaction rates, based on the most likely two-body energies. This also includes a necessary examination of the most likely excited states. Section V discusses limiting values of the basic physical parameters, and predicts Borromean structure and the related reaction mechanism at the astrophysical waiting points. This is combined to provide a method for estimating proton capture rates around the critical waiting points. Finally, we briefly summarize and conclude in Sec. VI.

II. THEORETICAL FRAMEWORK

Our aim is to calculate proton dripline three-body structures and capture rates from continuum two-proton states into the corresponding Borromean ground state at medium heavy waiting points. For this we need properties of ground and continuum states as well as the derived rates and cross sections. The general theoretical background can be found in Refs. [27–30], but for completeness we shall here collect the ingredients necessary to explain notation, calculations, and results. We shall only discuss two-proton three-body systems.

A. Three-body procedure

We outline briefly our method of hyperspheric adiabatic expansion of the Faddeev equations in coordinate space [27]. The system of two protons and a core can be described by three sets of the relative Jacobi coordinates, $(\mathbf{x}_i,\mathbf{y}_i)$, defined as

$$\mathbf{x}_i = (\mathbf{r}_j - \mathbf{r}_k)\sqrt{\frac{\mu_{jk}}{m}}, \tag{1}$$

$$\mathbf{y}_i = \left(\mathbf{r}_i - \frac{m_j\mathbf{r}_j + m_k\mathbf{r}_k}{m_j + m_k}\right)\sqrt{\frac{\mu_{jk,i}}{m}}, \tag{2}$$

$$\mu_{jk} = \frac{m_j m_k}{m_j + m_k}, \quad \mu_{jk,i} = \frac{m_i(m_j + m_k)}{m_i + m_j + m_k}, \tag{3}$$

where m is a normalization mass chosen to be the nucleon mass of 939 MeV$/c^2$. The six hyperspherical relative coordinates are the two pairs of directional angles, $(\Omega_{xi},\Omega_{yi})$, for $\mathbf{x}_i$ and $\mathbf{y}_i$, and hyperangle α_i and hyperradial ρ coordinates defined by

$$x_i = \rho\sin\alpha_i, \quad y_i = \rho\cos\alpha_i. \tag{4}$$

The Hamiltonian H can be written both in Jacobi and hyperspheric relative coordinates. For later convenience we focus here on the Jacobi set where $\mathbf{x}_{cp}$ connects core and proton, that is we can define

$$H = H_x + H_y + V_{pp}, \tag{5}$$

$$H_x = -\frac{\hbar^2}{2\mu_{cp}}\vec{\nabla}^2_{x_{cp}} + V_{cp}, \tag{6}$$

$$H_y = -\frac{\hbar^2}{2\mu_{cp,p}}\vec{\nabla}^2_{y_{cp,p}} + V_{cp'}, \tag{7}$$

where μ_{cp} and $\mu_{cp,p}$ are the reduced masses of core-proton and proton to core-proton systems, respectively. The three two-body interactions are the proton-proton interaction V_{pp}, the core-proton interaction V_{cp}, and the interaction between the core and the second proton, $V_{cp'}$. The coordinate dependencies of the two-body interactions, $V_{cp}(\mathbf{x}_{cp})$, $V_{cp'}(\mathbf{x}_{cp},\mathbf{y}_{cp})$, and $V_{pp}(\mathbf{x}_{cp},\mathbf{y}_{cp})$, between protons and core are given as arguments. In hyperspheric coordinates we have

$$T = -\frac{\hbar^2}{2\mu_{cp}}\vec{\nabla}^2_{x_{cp}} - \frac{\hbar^2}{2\mu_{cp,p}}\vec{\nabla}^2_{y_{cp,p}} = T_\rho + \frac{\hbar^2}{2m\rho^2}\Lambda^2, \tag{8}$$

$$T_\rho = -\frac{\hbar^2}{2m}\left(\frac{\partial^2}{\partial\rho^2} + \frac{5}{\rho}\frac{\partial}{\partial\rho}\right) = -\frac{\hbar^2}{2m}\left(\rho^{-5}\frac{\partial}{\partial\rho}\rho^5\frac{\partial}{\partial\rho}\right), \tag{9}$$

$$\Lambda^2 = -\frac{\partial^2}{\partial\alpha_i^2} - 4\cot(2\alpha_i)\frac{\partial}{\partial\alpha_i} + \frac{\hat{l}^2_{xi}}{\sin^2\alpha_i} + \frac{\hat{l}^2_{yi}}{\cos^2\alpha_i}, \tag{10}$$

where $\hat{l}_{xi}$ and $\hat{l}_{yi}$ are the angular momentum operators related to $\mathbf{x}_i$ and $\mathbf{y}_i$.

The method consists of an adiabatic expansion of the total wave function Ψ, that is

$$\Psi = \rho^{-5/2}\sum_n f_n(\rho)\Phi_n(\rho,\Omega), \tag{11}$$

where each of the angular wave functions Φ_n is a sum of Faddeev components, $\Phi_n = \phi_{n,1} + \phi_{n,2} + \phi_{n,3}$, related to the three corresponding Jacobi sets, and obeying the Faddeev equations

$$0 = (\Lambda^2 - \lambda_n)\phi_{n,i} + \frac{2m}{\hbar^2}\rho^2 V_i\Phi_n. \tag{12}$$

The angular eigenvalues, $\lambda_n(\rho)$, and the related complete set of eigenfunctions, Φ_n, are first computed for each ρ. Subsequently the radial expansion coefficients, $f_n(\rho)$, are found from the coupled set of radial equations

$$\left(-\frac{\partial^2}{\partial\rho^2} - \frac{2mE}{\hbar^2} + \frac{\lambda_n(\rho) + 15/4}{\rho^2} - Q_{nn}\right)f_n(\rho) = \sum_{n'\neq n}\left(2P_{nn'}\frac{\partial}{\partial\rho} + Q_{nn'}\right)f_{n'}(\rho), \tag{13}$$

$$P_{nn'} = \int \Phi_n^\dagger(\rho,\Omega)\frac{\partial}{\partial\rho}\Phi_{n'}(\rho,\Omega)\,d\Omega, \quad (14)$$

$$Q_{nn'} = \int \Phi_n^\dagger(\rho,\Omega)\frac{\partial^2}{\partial\rho^2}\Phi_{n'}(\rho,\Omega)\,d\Omega. \quad (15)$$

The left hand side reveals the crucial effective adiabatic part of the diagonal potential acting on the particles,

$$V_{\mathrm{eff},n} = \frac{\hbar^2}{2m}\left(\frac{\lambda_n(\rho)+15/4}{\rho^2}\right). \quad (16)$$

B. Potentials and properties

The result of the three-body calculations is dictated by the two-body potentials employed. The proton-proton interaction in free space is well known in many details and with high accuracy. However, its influence on the three-body solutions is only marginal provided; first of all, that the s-wave scattering length is reproduced, and second that the low-energy properties of the p and d partial waves are of reasonable (small) size and in fair agreement with the experimental values. The phenomenologically adjusted potentials described in Ref. [28] were used for the proton-proton interaction.

The test case used throughout this paper is the three-body system $^{68}\mathrm{Se}+p+p$ (^{70}Kr). However, the results apply to the region in general, as the small mass and charge variations between the three critical waiting points are inconsequential for our purposes.

The proton-core potential is on the other hand decisive and a careful choice has to be made. For light-to-medium heavy cores of mass numbers around 68 we use the Woods-Saxon form with a spin-orbit interaction, that is

$$V(r) = V_C(r) + \frac{V_0}{1+e^{(r-R)/a}} + \mathbf{l}\cdot\mathbf{s}\frac{1}{r}\frac{d}{dr}\frac{V_0^{ls}}{1+e^{(r-R_{ls})/a_{ls}}}, \quad (17)$$

where r is the distance between the two bodies, V_C is the Coulomb potential, V_0 and V_0^{ls} are the potential strengths of the nuclear and spin-orbit potential, $\mathbf{l}$ and $\mathbf{s}$ are the angular momentum and spin operators, and R and a are parameters governing the radius and the thickness of the potentials. This form is used for all partial waves, although the two strength parameters vary strongly depending mainly on the angular momentum.

A three-body potential will generally not be included. This would eventually be needed to adjust the energy levels according to a measured two- and three-body energy spectrum. However, the effect of such an addition is considered throughout the paper.

For the mass region in question we choose the values of the radial shape parameter to be $R = 7.2$ fm, $R_{ls} = 6.3$ fm, $a = 0.65$ fm, and $a_{ls} = 0.5$ fm. These choices are motivated by the knowledge of the average nuclear mean-field potentials and densities [31]. Accurate values are not needed because adjustments of the strengths in any case are necessary for fine-tuning the two-body energies. This is also one reason for omitting more complicated spin dependence like the tensor or quadratic spin-orbit potentials. In addition, the Coulomb potential is chosen from homogeneous charge distributions of radii, 5.6 fm, and 1.8 fm for core-proton system and proton-proton systems, respectively.

The two-body strength parameters are usually adjusted to reproduce the core-proton bound and resonance energies, but unfortunately the energy spectrum of ^{69}Br is not known experimentally. Based on shell model calculations the region is known to be near the midpoint of the fpg shell. The most likely two-body orbitals are then $f_{5/2}$, $p_{3/2}$ (or possibly $p_{1/2}$), and $g_{9/2}$. However, recent experiments show that the $g_{9/2}$ orbital is not important for nuclei around $A = 70$ with $N \simeq Z$ [32]. Instead f and p orbitals are assumed to dominate the low-lying spectrum. This is also confirmed by the known spectrum of the mirror nuclei [33]. To get opposite parity single-particle orbitals, necessary to form negative parity three-body states, a $d_{5/2}$ orbital can be included instead. To allow occupancy only of these selected two-body core-proton states in the three-body calculation is tricky because both lower- and higher-lying levels must be excluded. The Pauli forbidden two-body bound states are excluded for each partial wave by use of shallow potentials without bound states. The large-distance properties are then precisely correct but the unimportant nodes at small distances are then not present for these excited states.

To locate one and only one partial wave at a given small energy we must provide an accurately adjusted attractive potential, while all other partial waves must have sufficiently strongly repulsive potentials to prevent occupancy. A given two-body energy then provides one constraint correlating the two strengths. To select one and only one of two spin-orbit partners we choose a relatively high, positive or negative, value of V_0^{ls}. This may result in an abnormal order of spin-orbit partners, but the goal is achieved. The different partial waves are completely independent of each other on the two-body level, and we can therefore place all of them as we choose.

C. Radiative capture rate

We want to calculate the waiting time before two protons from the astrophysical environment are captured by a proton-dripline nuclear bound core. The reaction rate R for the corresponding one-step γ, three-body transition process, $p+p+c \to A+\gamma$, is given in general in Ref. [29]. For the special system of two protons plus an even-even core the rate becomes

$$R_{ppc}(E) = \frac{8\pi}{(\mu_{cp}\mu_{cp,p})^{3/2}}\frac{\hbar^3}{c^2}\left(\frac{E_\gamma}{E}\right)^2\sigma_\gamma(E_\gamma), \quad (18)$$

where $E_\gamma = E + B$ is the photon energy, E is the total three-body energy, and B is the three-body (positive) binding energy of the even-even nucleus A with the wave function Ψ_0. The photodissociation cross section $\sigma_\gamma(E_\gamma)$ for the inverse process $A+\gamma \to a+b+c$ is a sum over contributing electric multipole transitions of different orders, ℓ. That is

$$\sigma_\gamma^\ell(E_\gamma) = \frac{(2\pi)^3(\ell+1)}{\ell[(2\ell+1)!!]^2}\left(\frac{E_\gamma}{\hbar c}\right)^{2\ell-1}\frac{d}{dE}\mathcal{B}(\mathcal{E}\ell,0\to\ell), \quad (19)$$

where the strength function for the $\mathcal{E}\ell$ transition,

$$\frac{d}{dE}\mathcal{B}(\mathcal{E}\ell,0\to\ell) = \sum_i \left|\langle\psi_\ell^{(i)}||\hat{\Theta}_\ell||\Psi_0\rangle\right|^2\delta(E-E_i), \quad (20)$$

is given through the reduced matrix elements, $\langle\psi_\ell^{(i)}||\hat{\Theta}_\ell||\Psi_0\rangle$, where $\hat{\Theta}_\ell$ is the electric multipole operator, $\psi_\ell^{(i)}$ is the wave function of energy E_i for all bound and (discretized) three-body continuum states in the summation.

The astrophysical processes most often occur in a gas of given temperature T, which means we have to average the rate in Eq. (18) over the corresponding Maxwell-Boltzmann distribution, $B(E,T) = \frac{1}{2}E^2\exp(-E/T)/T^3$,

$$\langle R_{ppc}(E)\rangle = \frac{1}{2T^3}\int E^2 R_{ppc}(E)\exp(-E/T)\,dE, \quad (21)$$

where the temperature is in units of energy. Combining Eqs. (18)–(20) with Eq. (21) results in a full three-body calculation of the energy-averaged reaction rate, as the wave functions in Eq. (20) are proper three-body wave functions.

In the special case where the resonances are very narrow and well separated the expression can be simplified greatly. If $\psi_\ell^{(i)}$ is a bound state, or a very narrow resonance state described accurately as a bound state, we can assign a photon emission width Γ_γ to the transition from this state, that is given by [31]

$$\Gamma_\gamma = \frac{1}{2J+1}\frac{8\pi(\ell+1)}{\ell[(2\ell+1)!!]^2}\left(\frac{E_\gamma}{\hbar c}\right)^{2\ell+1}\left|\langle\Psi_0||\hat{\Theta}_\ell||\psi_\ell^{(i)}\rangle\right|^2, \quad (22)$$

where J is the angular momentum of the three-body resonance with energy E_R.

If furthermore the three-body resonance is approximated by a Breit-Wigner shape, the photodissociation cross section in Eq. (19) can be written as

$$\sigma_\gamma(E_\gamma) = \pi(J+1/2)\left(\frac{\hbar c}{E_\gamma}\right)^2\frac{\Gamma_{\rm eff}(E)\Gamma(E)}{(E-E_R)^2+\frac{1}{4}\Gamma(E)^2}, \quad (23)$$

where $[\Gamma_{\rm eff}(E)]^{-1} = [\Gamma_{ppc}(E)]^{-1} + [\Gamma_\gamma(E)]^{-1}$, Γ_{ppc} is the strong decay width, and the total (in principle energy dependent) width $\Gamma(E) = \Gamma_{ppc} + \Gamma_\gamma$.

With the dominating contributions arising from well separated, narrow resonances of Breit-Wigner shapes as in Eq. (22), the integral in Eq. (21) can be solved analytically, and we arrive at a very simple expression for the average rate:

$$\langle R_{ppc}(E)\rangle = \frac{4\pi^3(2\ell+1)\hbar^5}{(\mu_{cp}\mu_{cp,p})^{3/2}}\frac{\Gamma_{\rm eff}(E_R)}{T^3}\exp(-E_R/T). \quad (24)$$

The only assumption in this expression is that the photodissociation cross section is accurately expressed by the Breit-Wigner form in Eq. (22) with three-body resonance energy, $E_R \gg T$ and width $\Gamma \ll T$. Other contributing narrow well-separated resonances can simply be added. Thus Eq. (24) is valid for one or more contributing narrow resonance irrespective of capture mechanism.

The three-body (two proton plus an even-even core) calculation leads to a 0^+ ground state independent of the number and character of the contributing core-proton single-particle states. The lowest excited three-body bound or resonance state would almost definitely be a 2^+ state. This is confirmed by the mirror nuclei [34], where the two lowest excited states are 2^+ states. Furthermore, the lowest possibly negative parity state is 2.5 MeV above the ground state, and there is no 1^- at all in the known spectrum. The dominating transition can therefore be assumed to be an $\mathcal{E}2$ transition. To examine the remote possibility of a 1^- state two opposite parity single-particle states must be allowed. The relative energies of the 2^+ and 1^- states depend on the attractions of the two-body potentials for the corresponding partial waves. The energies of these excited states are, through Eq. (24), all-decisive for the capture rates. Besides the three-body resonance energy also the effective width $\Gamma_{\rm eff}$ is important for the capture rate. The realistic assumption that $\Gamma_{\rm eff} \approx \Gamma_\gamma$ allows an estimate of the relative sizes of the 2^+ to 1^- effective widths, that is from Ref. [31],

$$\frac{\Gamma_\gamma[\mathcal{E}(\ell+1)]}{\Gamma_\gamma(\mathcal{E}\ell)} \simeq \left(\frac{E_\gamma R}{\hbar c(2\ell+3)}\right)^2, \quad (25)$$

where R is the radius of the nucleus. For $\ell = 1$ we get with $E_\gamma = 1$ MeV and $R = 10$ fm that $\Gamma_\gamma(\mathcal{E}1) \approx 10^4\,\Gamma_\gamma(\mathcal{E}2)$. This estimate is from a single-particle model, but within the three-body model effects from the other proton can at most contribute by a factor of 2. The implication is that $\mathcal{E}1$ would dominate unless forbidden by rather strict conservation laws.

III. THREE-BODY GROUND STATE PROPERTIES

The nuclear properties of the waiting points are related to the Borromean structure reached after two-proton capture. We therefore first investigate the Borromean ground state depending on the two-body potentials varying along the proton dripline. In the following subsections we discuss three-body energies and structure of the corresponding wave functions.

A. Energies

The most tightly bound Borromean nucleus is most likely a closed (sub)shell for the core while the additional two protons occupy empty valence orbits. An extra stability is present for $N = Z$ nuclei which conveniently also includes waiting point nuclei for $N = Z = 32,34,36$. The ground states for both core and Borromean nuclei have zero angular momentum and positive parity as always for even-even nuclei. The first excited states of these nuclei are 0.9 MeV [35], 0.9 MeV [36], and 0.7 MeV [37], respectively. These rather high values demonstrate the stability required for a Borromean three-body structure built on these inert cores.

Given the significant Coulomb barrier the three-body system does in principle not need to be strictly bound. The only requirement is that the proton-decay branch is small compared to the β-decay branch. Small positive three-body energies are then possible, which in principle extends our energy region of interest. However, the β decay half life of ^{70}Kr has been measured to be 57(21) ms [38], so the possible extension is exceedingly small.

The two-body bound or resonance energies for the different partial waves are now the only pieces of information missing before the three-body properties can be calculated. We choose to use $p_{3/2}$ and $f_{5/2}$ and allow them both simultaneously with the same energy as well as one at a time. All other partial waves are either not present or shifted to high energies.

In Fig. 1 we show the lowest effective adiabatic potentials defined in Eq. (16) for the three cases with the same

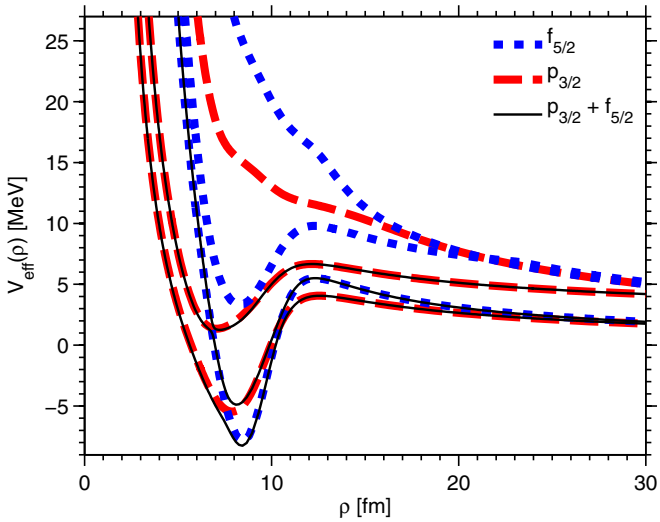

FIG. 1. The potentials based on the spectra of the lowest three λ's for $p_{3/2}$ (dashed red line) and $f_{5/2}$ (dotted blue line) in isolation, along with the combination of both $p_{3/2}$ and $f_{5/2}$ (solid black line). All two-body potentials have been adjusted to produce the energy $E_{2b} = 0.1$ MeV. It is seen how the spectrum of the combined case always follows the lowest available potential.

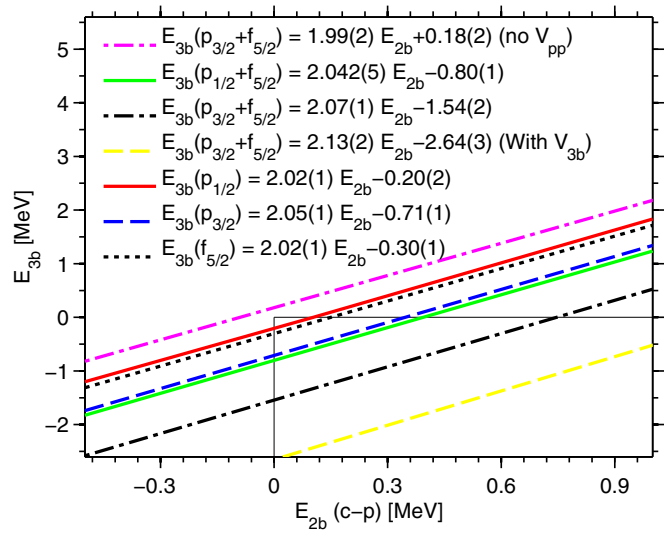

FIG. 2. The three-body energies as a function of two-body energies for $p_{1/2}$, $p_{3/2}$, and $f_{5/2}$ in isolation, and for $p_{1/2}$ and $f_{5/2}$ as well as $p_{3/2}$ and $f_{5/2}$ in combination, the latter both with and without p-p interaction, and with and without a three-body potential. The linear fits are in accordance with Eq. (29). All two-body potentials were adjusted to produce the same energy, when more that one wave is allowed. Only a 0^+ state is considered here. The horizontal and vertical line indicates our Borromean region of interest.

two-body energy, $E_{2b} = 0.1$ MeV, in all cases. We first notice an attractive potential for each contributing partial wave. When both $p_{3/2}$ and $f_{5/2}$ are allowed we find two attractive low-lying adiabatic potentials. Both contributions are present in the combined case where the deepest potential always follows the lowest potential from either $p_{3/2}$ or $f_{5/2}$ for different ρ values. Constructive (or destructive) interference can only marginally occur through nonadiabatic terms since p and f waves cannot couple to form a 0^+ state. However, this results in avoided crossings for the combined case which therefore must produce lower three-body energies than the individual cases. In general, the combined case can then never be less attractive than any of its components.

The coupled set of adiabatic radial potentials is solved and energies and wave functions calculated. The two-body input parameters are not known although limits from the required Borromean character can be found. We must therefore investigate the three-body properties as a function of the unknown two-body energies. The three-body energies E_{3b} are presented in Fig. 2 as functions of two-body energies E_{2b} for a various selection of contributing partial waves. The most spectacular observation is that all curves are linear. In the figure we only exhibit results for the most interesting energy interval but the same observed linear dependence is accurately followed within the investigated interval, -2.0 MeV $< E_{2b} < 2.0$ MeV.

When more than one partial wave is allowed, the two-body potentials are adjusted to produce the same energy. Fixing the energy of one two-body partial wave, while increasing another one from the same value, the E_{3b} must increase and approach the higher-lying curve corresponding to the one contributing wave. If more than two degenerate core-proton single-particle levels contribute we would find even lower-lying E_{3b} curves. However, this is highly unlikely since this requires nuclear potentials of unprecedented high symmetry. Omission of the proton-proton interaction in the case of two contributing partial waves, $p_{3/2}$ and $f_{5/2}$, increase the curve even above (0,0), which apart from center-of-mass effects should correspond to three noninteracting systems. Thus, we claim to have established limits for the E_{3b} variation between the lowest curve in Fig. 2 and a parallel curve roughly passing through (0,0).

So far, the results shown in Fig. 2 have been obtained using just the two-body interactions contained in Eqs. (5)–(7). However, it is a well known fact that using only two-body potentials will usually lead to an underbound three-body structure, as shown for instance for ^{17}Ne and ^{12}C in Refs. [23,39], respectively. This problem is typically overtaken by addition of an effective three-body force, $V_{3b}(\rho)$, to the adiabatic potential given in Eq. (16). Nevertheless, inclusion of such three-body force does not change the linear dependence shown in the figure. This is illustrated by the dashed (yellow) line in Fig. 2, which corresponds to the dot-dashed (black) case, but where a modest Gaussian three-body force $V_{3b}(\rho) = S_{3b}\exp[-(\rho/\rho_0)^2]$ has been included. In particular, the values $S_{3b} = -5.8$ MeV and $\rho_0 = 6$ fm have been used. As seen in the figure, inclusion of the three-body force only shifts the three-body energy, but keeps the energy relation intact.

B. Structure

The simple linear dependency in Fig. 2 is due to the special structure of the wave function and the Hamiltonian in Eq. (5). The core is much heavier than the proton, and the reduced masses are to a very good approximation both equal to the

proton mass. Then $x_{cp} \approx y_{cp}$ and the Hamiltonians in Eqs. (6) and (7) are also approximately equal, $H_x \simeq H_y$. If $|\Psi_{3b}\rangle$ denotes the three-body wave function, the three-body energy is determined as the expectation value of the Hamiltonian in Eq. (5), that is

$$E_{3b} = \langle\Psi_{3b}|\, H_x\, |\Psi_{3b}\rangle + \langle\Psi_{3b}|\, H_y\, |\Psi_{3b}\rangle + \langle\Psi_{3b}|\, V_{pp}\, |\Psi_{3b}\rangle \simeq 2E_x + E_{pp}, \tag{26}$$

where the approximate equality arises due to the assumption $x_{cp} \approx y_{cp}$. This approximation is consistent with $|\Psi_{3b}\rangle$ as a product of corresponding two-body wave functions. For instance, when two single-particle states are allowed, for example $p_{3/2}$ and $f_{5/2}$, we have $|\Psi_{3b}\rangle = A\,|p_{3/2}\rangle_x\,|p_{3/2}\rangle_y + B\,|f_{5/2}\rangle_x\,|f_{5/2}\rangle_y$, where the angular momentum coupling to 0^+ of both terms implicitly is assumed. Product terms of $p_{3/2}$ and $f_{5/2}$ are not allowed because the total angular momentum 0^+ cannot be reached.

The above product structure of $|\Psi_{3b}\rangle$ is rather general, since the $\mathbf{x}_{cp}$ distribution necessarily is described by the allowed single-particle wave functions whereas the same overwhelmingly dominating single-particle $\mathbf{y}_{cp}$ part for completeness should be extended to include other angular momentum components. We then get

$$E_x = \langle\Psi_{3b}|H_x|\Psi_{3b}\rangle = A^2E_{2b}(p) + B^2E_{2b}(f), \tag{27}$$

where the two-body energies are defined by

$$E_{2b}(p) \equiv \langle p_{3/2}|H_x|p_{3/2}\rangle_x\,, \qquad E_{2b}(f) \equiv \langle f_{5/2}|H_x|f_{5/2}\rangle_x\,, \tag{28}$$

and the cross terms vanish both due to orthogonality of the eigenfunctions of H_x and angular momentum conservation of the Hamiltonian. We then arrive at the estimate of the three-body energy

$$E_{3b} \simeq 2[A^2E_{2b}(p) + B^2E_{2b}(f)] + \langle\Psi_{3b}|V_{pp}|\Psi_{3b}\rangle\,, \tag{29}$$

where $A^2 + B^2 = 1$. The occupation probabilities A^2 and B^2 are given by the relative weights of the partial waves. If only $p_{3/2}$ or $f_{5/2}$ are allowed we have $A = 1$ and $B = 0$ or $A = 0$ and $B = 1$, and consequently the linear dependence seen in Fig. 2. If $E_{2b}(p) = E_{2b}(f)$ the linear dependence still results, and in both extremes the slopes of the curves are 2. Variation between limits must produce a curve connecting the corresponding two lines. For example, the lower limit, when allowing both $p_{3/2}$ and $f_{5/2}$, is given by the black, dash-dotted line, and the upper limit is given by the curve corresponding to the wave with lowest energy. We emphasize the remarkable equality of the slopes of the lines in Fig. 2.

The structure of the solutions is quantified by decomposition into contributing partial waves. We collect the results in Table I for the same seven cases as seen in Fig. 2 with both sets of Jacobi coordinates. We have chosen two rather different values, −2.0 and 2.0 MeV, for the two-body energies used to adjust the strength parameters. The distributions are very similar for the two energies, and the transition from one distribution to the other is slow and monotonous. Adding a three-body potential has no significant effect on the structure of the wave function.

TABLE I. The weights of each partial wave for the same cases as shown in Fig. 2. The state in question is a 0^+ state. Here l_x denotes the relative angular momentum between the two particles specified by the second column, l_y denotes the angular momentum of the third particle relative to the center of mass of the first two particles, and l_t is the total angular momentum they combine to. The sixth column gives the order $K_{\max}$ of the Jacobi polynomium used for the corresponding partial wave. The last two columns shows the weight (in percent) of the states for different two-body c-p energies. Components where all states have a weight less than 10% are generally not included.

Waves	Jacobi	l_x	l_y	l_t	$K_{\max}$	E_{2b} (MeV)	
						−2.0	2.0
$p_{3/2}$	p-p	0	0	0	98	78	76
		1	1	1	80	20	22
	p-c	1	1	0	80	79	77
		1	1	1	80	20	23
$p_{1/2}$	p-p	0	0	0	98	48	45
		1	1	1	80	49	52
	p-c	1	1	0	80	49	46
		1	1	1	80	51	54
$f_{5/2}$	p-p	0	0	0	98	48	47
		1	1	1	80	37	38
		2	2	0	52	11	11
	p-c	3	3	0	74	60	59
		3	3	1	74	40	41
$p_{3/2} + f_{5/2}$	p-p	0	0	0	98	78	75
		1	1	1	80	19	22
	p-c	1	1	0	80	56	52
		1	1	1	80	12	13
		3	3	0	74	23	24
		3	3	1	74	9	11
$p_{3/2} + f_{5/2}$ ($V_{3b} \neq 0$)	p-p	0	0	0	98	80	77
		1	1	1	80	18	20
	p-c	1	1	0	80	62	57
		1	1	1	80	13	13
		3	3	0	74	19	21
		3	3	1	74	6	9
$p_{3/2} + f_{5/2}$ ($V_{pp} = 0$)	p-p	0	0	0	98	65	64
		1	1	1	80	33	32
	p-c	1	1	0	80	66	65
		1	1	1	80	34	33
		3	3	0	74	0	0
		3	3	1	74	0	0
$p_{1/2} + f_{5/2}$	p-p	0	0	0	98	66	61
		1	1	1	80	31	35
	p-c	1	1	0	80	38	34
		1	1	1	80	20	21
		3	3	0	74	30	31
		3	3	1	74	11	14

The decomposition is rather trivial, when only one single-particle orbit is allowed. In the second set of Jacobi coordinates, the proton-core set, only this state is allowed. However, two couplings to total orbital angular momentum, $l_t = 0$ and 1, share the weights, which is equally distributed in the first Jacobi set since l_t is conserved in this rotation.

When two single-particle orbits are allowed the decomposition includes both structures with different relative weights.

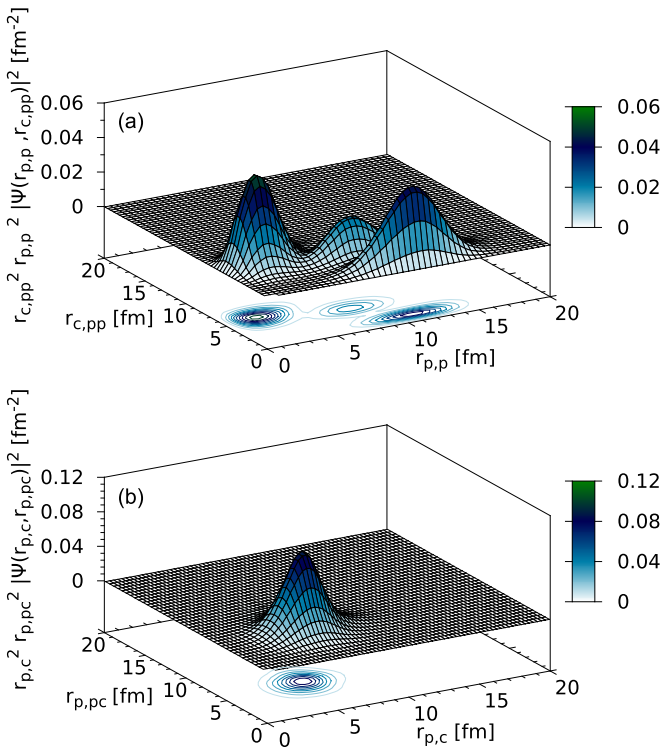

FIG. 3. The probability distribution for the 0^+ ground state with equal two-body binding of 0.641 MeV for both $f_{5/2}$ and $p_{3/2}$ partial waves. Projected contour curves are shown at the bottom of each figure. The distance variables correspond to the two different Jacobi sets, where panels (a) and (b) are for the first and second Jacobi sets, respectively.

The $l_t = 0$ components are always far larger than those of $l_t = 1$. The distribution is strongly depending on the proton-proton interaction as seen by the complete separation for $V_{pp} = 0$, where the three-body ground state is degenerate corresponding to either $|p_{3/2}\rangle_x\,|p_{3/2}\rangle_y$ or $|f_{5/2}\rangle_x\,|f_{5/2}\rangle_y$.

As seen from Eq. (29) the displacement of the lines in Fig. 2 not only depends on the proton-proton interaction, but also on the wave function. The spin-orbit difference between $p_{1/2}$ and $p_{3/2}$ causes a slightly different wave function, which is why the two curves differ. This is also demonstrated by the fact that displacement changes from -1.54 to 0.18 MeV, when a very shallow nuclear potential and neither spin-spin, spin-orbit, tensor, or Coulomb potentials are used in the proton-proton interaction. In fact, by completely eliminating the proton-proton interaction, the result is almost two independent two-body systems. The slight positive displacement is in that case due to the fact that all three coordinates $\mathbf{r}_1$, $\mathbf{r}_2$, and $\mathbf{r}_3$ are still coupled in the $\mathbf{y}$ coordinate as long as the core is not infinitely heavy.

The actual size of the displacement, caused by the proton-proton interaction, can in principle be estimated from the matrix element $\langle\Psi|V_{pp}|\Psi\rangle$. We show the probability distribution of the three-body wave function in Fig. 3 where the distance of about 5 fm between proton and core [Fig. 3(b)] is a prominent feature. The proton-proton distance distribution [Fig. 3(a)] is much more complicated with three peaks at distances of about 2.5, 8, and 11 fm, respectively. The Coulomb repulsion would correspondingly be about 0.6, 0.18, and 0.13 MeV.

The strong nucleon-nucleon interaction has strength of around 40 MeV and range of 2 fm. To arrive at a total displacement of around -1.7 MeV there must be only a few percent of the proton-proton distance-probability within the range of 2 fm. To make a reliable estimate of the displacement is therefore very delicate as it depends strongly on the solution to the three-body problem. A much better computation would be to evaluate E_{pp} directly. However, this would still be only an estimate since Ψ changes with the interaction, and at best we can only reproduce the already known actual curves in Fig. 2.

IV. RADIATIVE CAPTURE

The critical waiting points in the rp process are defined by the long time it takes to capture an additional two protons in the nucleus. The Borromean nature requires a three-body reaction producing the strong interaction bound two-proton plus core system. In this section we shall focus on corresponding reaction rates and the structure of crucial intermediate states. The total process is $c + p + p \rightarrow A + \gamma$, which as well can be understood through the reverse process, $A + \gamma \rightarrow c + p + p$. It is often very accurate to divide part of this process into two steps, $A^* \leftrightarrow A + \gamma$, where A^* is one (and sometimes a few) intermediate excited state. We shall first investigate the properties of such intermediate excited states and subsequently calculate the reaction rates. Unless otherwise stated a two-body energy of 0.641 MeV is used, as this is the measured proton separation energy of ^{69}Br [40]. The results are not restricted to such a specific energy, but apply rather generally to the region of the nuclear chart around the critical waiting points.

A. Excited continuum states

The reactions proceed from continuum three-body states, that is from two free protons and an (almost) ordinary nucleus. This problem can be handled by two conceptually different methods [39,41], where the first is to specify the boundary conditions directly and solve the Schrödinger equation. The second method is to discretize the continuum in a large hyperradial box which in the present case is limited by hyperradii less than the box radius $\rho_{\max}$.

We shall here use the discretization method with the great advantage of using the already defined adiabatic potentials. As discussed in Sec. II C the most likely dominating intermediate angular momenta is 2^+. Also, as discussed in Sec. II B, states with the necessary opposite parity to form a 1^- state is also very unlikely. However, to later study the scale of the $\mathcal{E}1$ transition, $p_{3/2}$ and $d_{5/2}$ waves are allowed to form a 1^- state. We show the lowest corresponding adiabatic potentials in Fig. 4 for three such cases, where two partial waves for each total angular momentum are allowed. The parameters are chosen to be the same as already used in the study of ground state properties.

The potentials in Figs. 4(a) and 4(b) are qualitatively similar to those of Fig. 1 with attractive pockets around $\rho = 8$ fm, infinite repulsion at smaller distances, and barriers at larger ρ separating regions of interacting and fully separated three

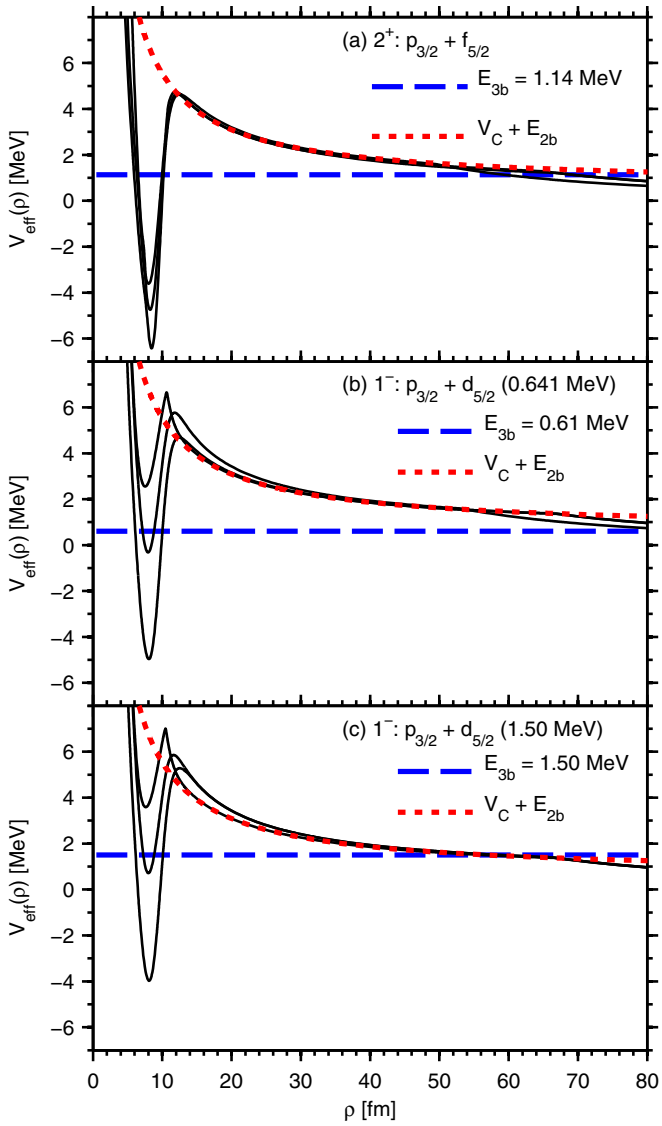

FIG. 4. (a) The potentials based on the spectra of the lowest five λ's for the 2^+ state allowing both $p_{3/2}$ and $f_{5/2}$ waves. The dashed, horizontal line is at the lowest three-body resonance energy. The dotted curve is the sum of Coulomb potential and two-body energy. (b) The same for the 1^- state with $p_{3/2}$ and $d_{5/2}$ waves. (c) The same as for (b) with the $d_{5/2}$ two-body energy equal to 1.5 MeV.

particles. The attractive region and the substantial barrier suggest that there are narrow, low-lying resonances or perhaps even bound states. The energies of the radial solutions in the box are at first glance also similar to the ground state 0^+ solutions, that is one prominent bound, separate, low-lying state and a number of higher-lying solutions. However, the bound solutions have positive energy and would therefore correspond to resonances or continuum states. The 1^- potentials shown in Fig. 4(c) are much more repulsive at short distances since the necessary $d_{5/2}$ state is chosen to be at 1.50 MeV. The resonance is at a higher energy, where also more continuum background states have a nonvanishing contribution at short distances.

The three-body energy for the 1^- case with $E_{2b}(p) \neq E_{2b}(d)$ can be explained using an argument similar to that

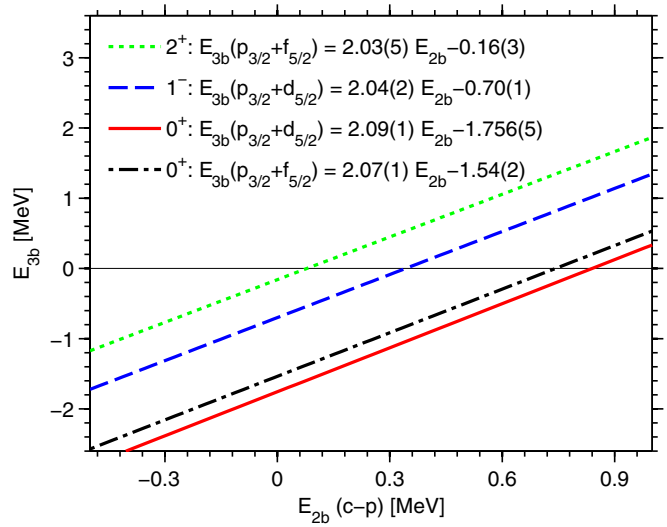

FIG. 5. The three-body energy as a function of two-body energy for the 0^+ and 2^+ state with $p_{3/2}$ and $f_{5/2}$ waves, as well as for the 0^+ and 1^- state with $p_{3/2}$ and $d_{5/2}$ waves. The horizontal line is included to guide the eye.

in Sec. III B. The three-body wave function can be written as $|\Psi_{3b}\rangle = A\,|p_{3/2}\rangle_x\,|d_{5/2}\rangle_y + B\,|d_{5/2}\rangle_x\,|p_{3/2}\rangle_y$, where the angular momentum coupling is to 1^-. As $m_c \gg m_p$ the likely weight of the two configurations must be the same, and since these are the only possibilities we have $A^2 = B^2 = 1/2$. Then $E_x = 1/2[E_{2b}(p_{3/2}) + E_{2b}(d_{5/2})]$, and $E_{3b} = E_{2b}(p_{3/2}) + E_{2b}(d_{5/2}) + E_{pp}$. It was found that if $E_{2b}(p_{3/2}) = E_{2b}(d_{5/2}) = 0.641$ MeV then $E_{3b} = 0.61$ MeV, which means $E_{pp} \sim -E_{2b}(p_{3/2})$ for that specific energy. However, the three-body wave function is almost unchanged when changing $E_{2b}(d_{5/2})$ because both the p and d wave is needed to form the 1^- state, and E_{pp} is therefore also almost unchanged. The result is $E_{3b} \simeq E_{2b}(d_{5/2})$ for $E_{2b}(p_{3/2}) = 0.641$ MeV.

The three-body large-distance configuration is also revealed by close inspection of Fig. 4. A region around $\rho = 40$–50 fm is seen where one potential tends to be more flat than dictated by a general Coulomb decreasing potential. The size and slow decrease is precisely consistent with the Coulomb potential between one proton and a proton-core two-body system in a spatially small resonance at 0.641 MeV. This is reflected in the good agreement between the lowest potential and the corresponding Coulomb potential plus two-body energy seen in Fig. 4. In Fig. 4(c) the same $V_C + E_{2b}$ barrier is indicated by the red, dotted curve. This implies that the close-lying proton is in a p orbital.

The three-body (bound) resonance energies are not necessarily the lowest discretized states. It depends strongly on the size of the box since an infinite box must produce a continuum of states from the threshold and upwards. We detect the resonance state by requiring that the density distribution is localized at small distances. The resonance energies are shown in Fig. 5 as function of two-body energies for the choices used for the ground state calculations. It is perhaps less surprising to find the same simple and accurate linear dependence as we observed for the ground states. The criteria for linearity are the

TABLE II. The weights of each partial wave for the 2^+ case, where only $p_{3/2}$ and $f_{5/2}$ waves are allowed, and for the 1^- case, where only $p_{3/2}$ and $d_{5/2}$ waves are allowed. The notation is the same as in Table I. The last three columns shows the weight (in percent) of the lowest resonances. The resonances correspond to the first peaks in Fig. 6. Components where all states have a weight less than 10% are not included.

Waves	Jacobi	l_x	l_y	l_t	$K_{\max}$	Weight		
2^+	p-p	0	2	2	199	27	8	15
$p_{3/2} + f_{5/2}$		1	1	1	199	40	11	11
		1	1	2	199	3	19	2
		1	3	3	202	1	17	12
		2	0	2	60	23	8	13
		3	1	3	22	1	17	12
	p-c	1	1	1	160	41	12	10
		1	1	2	160	38	4	1
		1	3	2	162	3	15	15
		1	3	3	162	1	20	23
		3	1	2	162	3	15	15
		3	1	3	162	1	20	23
2^+	p-p	0	2	2	199	23	25	
$p_{3/2}$		1	1	1	199	53	41	
		2	0	2	60	21	24	
	p-c	1	1	1	200	55	42	
		1	1	2	200	45	52	
1^-[a]	p-p	0	1	1	199	66		
$p_{3/2} + d_{5/2}$		1	0	1	199	13		
	p-c	1	2	1	161	38		
		2	1	1	161	38		
1^-[b]	p-p	0	1	1	199	66		
$p_{3/2} + d_{5/2}$		1	0	1	199	14		
	p-c	1	2	1	161	38		
		2	1	1	161	38		

[a] $E_{2b}(p_{3/2}) = E_{2b}(d_{5/2}) = 0.641$ MeV.
[b] $E_{2b}(p_{3/2}) = 0.641$ MeV, $E_{2b}(d_{5/2}) = 1.50$ MeV.

same. Also the effect of a three-body potential would be similar to the effect seen in Fig. 2 only it would be more difficult to justify the exact size of the potential as the excitation spectrum is less well known.

We can then conclude that the excitation energy is a constant independent of the chosen variation in Figs. 5 and 2. Specifically we get excitation energies 1.38 and 1.06 MeV for the 2^+ and the 1^- states, respectively. However, the derived limits of variation are completely different. The 2^+ excitation energy is strongly limited, since the ground state only can move between finite limits as shown in Fig. 2, and the lowest 2^+ resonance is entirely determined by the $p_{3/2}$ component even when also $f_{5/2}$ is allowed with the same energy as seen in Table II.

The reason for this behavior is that any partial wave (except angular momentum 1/2) of proton and 0^+-core states can be occupied by two protons coupled to both 0^+ and 2^+. The excitation energy can then vary at most by about 1.5 MeV. In contrast, the 1^- state requires both positive and negative parity proton-core single-particle states. Thus, a well defined finite 0^+ ground state energy always appears whereas the 1^- excitation energy can vary from zero to infinity by increasing one of the necessary proton-core states towards infinity.

The discretization allows normalization of all the states in the box. Specifically, as mentioned above the density distributions of the resonance states are localized at small distances. The probability distributions are almost indistinguishable from that of Fig. 3 each with a peak at a proton-core distance of about 6 fm. Only one 1^- resonance is found whereas three rather pronounced low-lying 2^+ resonances appear when both $p_{3/2}$ and $f_{5/2}$ are allowed with the same energies. By definition all these states have the overwhelmingly large probability located at small distances. The spatial overlaps with corresponding ground states are therefore very large in all theses cases. Thus, only appropriate angular momentum dependent operators and resonance energies are required to initiate highly likely transitions, as seen in Eq. (19).

It is then important to know the angular momentum composition of the excited states. The choices of allowed partial waves are strongly limiting for these distributions as seen in Table II. The simplest are the lowest 2^+ state and the 1^- resonance. They consist of only proton-core $p_{3/2}$ components, and equal measures of proton-core and $p_{3/2}$-$d_{5/2}$ components, respectively. The two excited 2^+ states are mixtures of $p_{3/2}$ and $f_{5/2}$ proton-core partial wave components.

All discretized continuum states, beside the resonances discussed above, are much more dilute and spread out at large distances of the box. The spatial overlaps with the ground state are therefore very small and any transitions would correspondingly be reduced in size. This does not necessarily mean that their contributions can be ignored, because the number of these states also increase both with box size and with energy. At some point they overlap and contribute as a genuine continuum.

B. Cross section and reaction rates

The three particles in the continuum are not characterized by one complete set of quantum numbers. The plane wave states for free particles contain all angular momenta in a partial wave expansion. In contrast the final nuclear state has given angular momentum and parity, and the transition itself is conveniently specified by a given one-body multipole operator. The transitions between well defined states are independent of each other, and the prescription is therefore to calculate and add the different contributions. The transition probabilities decrease strongly with multipolarity, which therefore is decided by nature through the structure of the Borromean final state.

The 0^+ quantum numbers are achieved by coupling of the two proton-core angular momenta, which must be unoccupied by core nucleons. The available low-lying single-particle orbits therefore depends entirely on the region of interest in the nuclear chart. We focus on the proton dripline region around $A = 68$, and as discussed $f_{5/2}$ and $p_{3/2}$ are from the mirror nuclei expected to be the dominating single-particle orbitals, with $\mathcal{E}2$ being the dominating transition. For completeness we shall nevertheless investigate the heavily suppressed $\mathcal{E}1$ transition.

We proceed by calculating the discretized three-body continuum states for given total angular momentum and parity

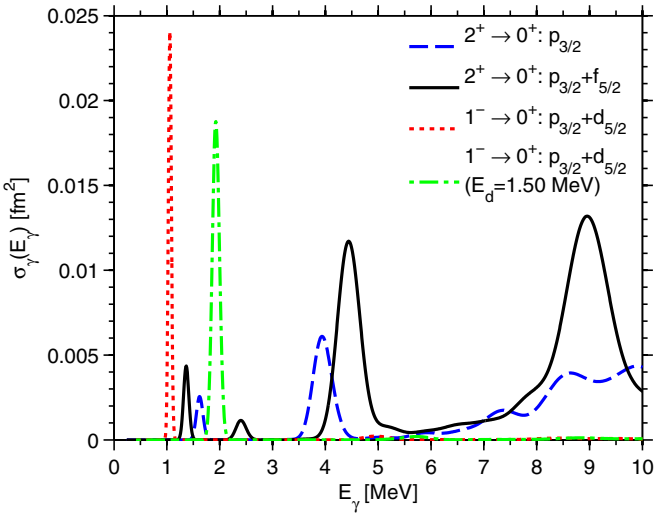

FIG. 6. The cross sections for $2^+ \to 0^+$ with both $p_{3/2}$ and $f_{5/2}$ waves (solid, black curve), and only with $p_{3/2}$ waves (dashed, blue curve). Also included are the cross section for $1^- \to 0^+$ with $p_{3/2}$ and $d_{5/2}$. For the red dotted curve $E_{d_{5/2}} = 0.641$ Mev, and $E_{d_{5/2}} = 1.50$ MeV for the green dash-dotted curve. In both cases the $\mathcal{E}1$ transition has been scaled down by 10^3 to make the figure readable. The photodissociation energy is related to the total energy E and the binding energy B by $E_\gamma = E + |B|$.

with selected two-body input energies. The cross sections and reaction rates can then be obtained by summation over these discrete "continuum" states. The method does not assume any specific reaction mechanism, that is two-step via a photon emitting resonance and/or continuum state, and both sequential and direct reactions are included in the numerically obtained results.

The discretization implies that the low-energy spectrum can be too sparse when the box size is comparable to the extension of the potential barriers. The space outside the barriers is then too small to provide box bound states. On the other hand, an attractive short-distance pocket would produce an isolated bound-state like resonance which then would mediate all the low-energy transition probability. The missing continuum states in its energy neighborhood would have vanishing spatial overlap with the ground state, and consequently also vanishing transition probability. In the high-energy limit the level density increases and the contributions are distributed over many levels. At some point the included Hilbert space in the basis becomes insufficient. Fortunately, we are able to cover an energy region sufficient for the astrophysical reactions of interest.

In Fig. 6 we show the cross section from Eq. (19) as function of energy above threshold for two cases of 2^+ and 1^- excitations each. All the peaks are at the resonance energies where the spatial overlaps to the ground state allow finite cross sections. Two clear differences are seen between the two 2^+ cases. First of all, the two lowest $p_{3/2} + f_{5/2}$ peaks are pushed a little bit further apart as for a two-level system with an additional interaction. Second, the peaks are notably smaller when only $p_{3/2}$ is allowed. The reason is the partial wave composition of the peaks and the number of contributing potentials.

All peaks are in the $p_{3/2}$ case composed entirely of $(l_x,l_y) = (1,1)$, as seen in Table II, where only one potential contributes significantly to the lowest peak. In the $p_{3/2} + f_{5/2}$ case the same structure is found in the lowest peak where two potentials now contribute evenly. The next two peaks are in contrast composed of an almost even mixture of $(l_x,l_y) = (1,3)$ and $(3,1)$, which clearly is not allowed with only the contribution from the $p_{3/2}$ state. In between the resonance peaks are the part of the cross section which makes the nonresonant contribution to the reaction rate. This contribution is completely negligible compared to the resonant contribution for low energies while increasingly appearing at higher energies. As the lowest peak consists almost exclusively of p waves, adding higher angular momentum orbitals would not change the cross section nor the resulting reaction rates.

The cross section for the 1^- excitation is also shown in Fig. 6. When the $d_{5/2}$ and $p_{3/2}$ two-body states have the same energy we find only one huge contribution at very low energy corresponding to one and only one resonance. When the $d_{5/2}$ energy is increased this cross section peak (resonance energy) moves up in energy, gets broader, and decreases in size. It is found that increasing the $d_{5/2}$ energy to 3.00 MeV makes the $\mathcal{E}1$ contributions insignificantly small compared to the $\mathcal{E}2$ contributions in Fig. 6. We can conclude that $\mathcal{E}1$ transitions are large even for relatively high-lying two-body states which are necessary for the composition of the 1^- continuum or possible 1^- resonances.

The capture process takes place in an environment where temperature is an important parameter. The three-body energy is therefore not *a priori* given, but occurs with a certain probability distribution and with the capture rate specified in Eq. (21). The resulting rates are given by the full lines in Fig. 7. The lowest resonance peaks in Fig. 6 suggest narrow states, which can be approximated by a Breit-Wigner shape. It is then possible to use the much simpler expression in Eq. (24) to find the contribution from each resonance to the overall reaction rate.

Figure 7 shows that the lowest resonance clearly dominates for both cases even at temperatures well above 3 GK. Summing the contribution from the isolated lowest resonances results in a better agreement with the full calculation to a higher temperature, but large deviations appear above around 5 GK. It is very remarkable that such a simple expression, based on a single resonance, is able to estimate the reaction rate so accurately over several GK. It is even more impressive that a simple sum over the resonances can further increase the temperature range of its applicability while maintaining the accuracy. Increasing the $d_{5/2}$ energy increases the resonance energy, which in turn increases the temperature with the highest rate, while simultaneously reducing this rate. The characteristic peak in the reaction curve is also smeared out by the effects of higher energy continuum contributions.

There are a number of possible corrections, which should be considered. First of all, the rates in Fig. 7 are based on the full three-body 2^+ (1^-) spectrum in the energy region seen in Fig. 6. If, as in the mirror nuclei [34], several of the lowest states are 2^+ states, they are all included. Contributions from

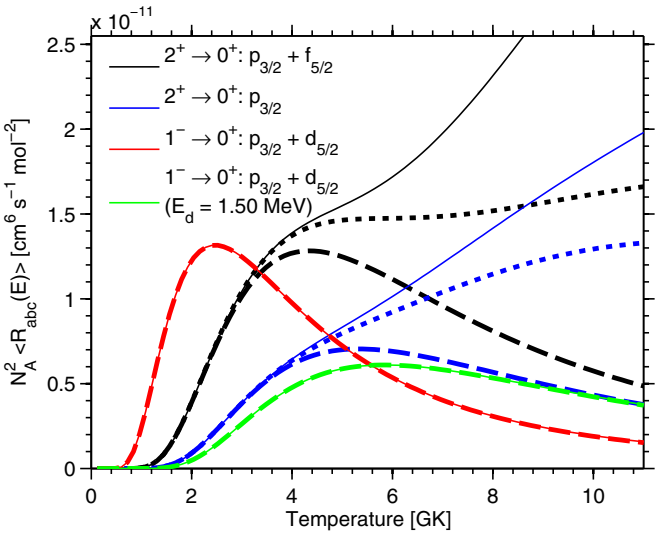

FIG. 7. The reaction rates corresponding to the cross sections from Fig. 6. The result of the full calculations is given by the solid curves. The dashed curves in the same color are the result of applying Eq. (24) to the lowest peak in Fig. 6. The dotted curves are the sum of contributions for the three (two) lowest resonances for $p_{3/2} + f_{5/2}$ ($p_{3/2}$) using Eq. (24). The $\mathcal{E}1$ rates have been scaled down by 10^4 to make the figure readable. The various resonance widths for the lowest resonances can be found in Table III.

other possible states, such as 4^+ or 3^- states, could conceivably contribute, but they would be suppressed by several orders of magnitude because of the higher order transition necessary. All transitions are to the same 0^+ ground state. Excited, bound three-body states are not accounted for as they are very unlikely at the edge of the dripline, in particular considering the lowest excited state in the mirror nuclei is 0.94 MeV above ground [34].

Due to the high temperatures involved core excitations could also be a contributing factor. The first excited state in ^{68}Se is $E_{c1} = 0.854$ MeV above the ground state [36]. The probability of occupation at a temperature of 4 GK would then be $\exp[-E_{c1}/(k_B T)] = 0.09$. To get the reaction rate from Eq. (21) we must multiply by R_{cpp} which is proportional to the photodissociation cross section as parametrized in Eq. (23) for a resonance. The peak structure suggested by the parametrization is used to derive Eq. (24) which assumes that the barrier penetration factor contained in Γ and $\Gamma_{\rm eff}$ has a relatively smooth energy dependence. The numerical calculations of σ_γ shown in Fig. 6 reveal the expected peak structure for small E_γ confirming the sufficient smoothness of Γ and $\Gamma_{\rm eff}$. With everything being the same for ground and excited states we conclude that the contribution from low-lying excited states are reduced by their Boltzmann factor which then would be only a minor contribution. The second excited core state is 1.20 MeV above ground, and is even less significant. To include contributions from core excitations or other bound three-body states one would have to include the partition functions of both the initial target and final three-body nucleus [5,42], to account for the thermal equilibrium between the ground and the excited states. This would in this case be minor corrections.

The discretized three-body states are limited to energies less than 10 MeV, so the rates must decrease for sufficiently high temperatures. Going to higher temperatures the computed $\mathcal{E}2$ transition rate has a maximum value of about 6.5 and $3.5 \times 10^{-11} N_A^2$ cm^6 s^{-1} mol^{-2} at just above 25 GK for the black and the blue curve respectively, and then decreases similarly to the $\mathcal{E}1$ transition. The maximum value for the $\mathcal{E}1$ transition occurs at much lower temperatures as there is, as seen from Fig. 6, no significant contribution to the cross section at higher energies. In both cases, the restriction imposed by the limit in discretized energies is only relevant far outside our region of interest.

As the single peak approximation fails at higher temperatures it would also fall short at lower temperatures. At low temperatures even the lowest resonance state would not have a significant probability of being populated, and the rate would be dominated by off-resonance contributions. Fortunately, this is well below our region of interest.

If both a 2^+ and a 1^- state was present simultaneously transitions like $2^+ \to 1^- \to 0^+$ or $1^- \to 2^+ \to 0^+$ could be imagined, which would affect the final reaction rate. This effect could be computed by establishing the relations between the relevant two- and three-body energies, and then calculating the reaction rate in the same way as before. As before, the effect of any higher-lying resonances would only be significant if the temperature was sufficiently high, as demonstrated by the accuracy of the lowest peak in isolation in Fig. 7. For our purposes it is therefore unnecessary to consider such corrections.

If a three-body force is added and the energy levels shifted, the effect on the cross section and reaction rate is only an energy scaling determined by Eqs. (19) and (24) respectively. The overlap matrix element would not change, as the energy shift does not change the structure of the wave function as seen from Table I.

V. PRACTICAL IMPLICATIONS

The formulations and calculations presented in the previous sections are schematic or quantitatively accurate depending on the point of view. The schematic impression arises from the relatively strong assumptions of the few contributing proton-core partial waves. This is, however, not unrealistic within the field of few-body cluster models, which has also been able to provide an appropriate description of two weakly bound nucleons surrounding an ordinary nuclear core. The quantitative accuracy emerges as soon as the few-body model approximations are shown to be correct, because then the reliability and completeness of the results are unavoidable.

The final purpose of this paper is to provide a method for estimating proton capture reaction rates for the region around $A \sim 70$ and $N \sim Z$ in general, and the critical waiting points in particular. To that end we first discuss the reaction mechanism resulting from the sets of input parameters. Second, we present estimates of the crucial two-and three-body ground and first excited state energies, and finally, we combine these considerations to present a general method for estimating radiative capture rates around the critical waiting points.

A. Reaction mechanism

The calculations are carried out without need for specification of the reaction mechanism. In contrast, from the calculated results we can deduce how the process proceeds between the Borromean bound state and the three free constituents in the continuum. Due to the principle of detailed balance both reaction directions are equally well suited for both qualitative and quantitative descriptions. In words the process starts with bombarding the Borromean bound state with photons of energy larger than the three-body binding energy, where the populated continuum states somehow end up as three independent infinitely separated three particles, that is two protons and a core.

The process $A + \gamma \rightarrow p + c + p$ could proceed in several possible steps. It could include an excited continuum state of the Borromean nucleus, A^*, or a quasistable two-body proton-core (pc) configuration, although either or both of these steps might be skipped. In this way the process is divided in distinct, and possibly, independent steps. Whether they are followed or not in a sequential progression is defining the reaction mechanism, and is used to categorize it.

The traditionally denoted sequential path [43,44] is with the proton-core state, but with or without A^*,

$$A + \gamma \rightarrow A^* \rightarrow (pc) + p \rightarrow p + c + p,$$
$$A + \gamma \rightarrow (pc) + p \rightarrow p + c + p.$$

Likewise, the route usually called direct [10,44], again with or without A^*, is

$$A + \gamma \rightarrow A^* \rightarrow p + c + p,$$
$$A + \gamma \rightarrow p + c + p.$$

The path chosen by nature depends on the characteristics of the system. However, substantial numerical simplifications as well as insight can be gained with a dominating narrow resonance. Approximating the cross section by a peaked function like a Breit-Wigner shape we arrive at the extremely simple temperature dependent rate expression in Eq. (24). This is exactly the same expression as in Eq. (15) of Ref. [30], with Γ_γ replaced by $\Gamma_{\rm eff}$. However, in Ref. [30] this reaction rate is derived in the "extreme sequential limit," under the much stronger conditions that Γ_γ is much smaller than Γ_{ppc}, and the direct decay is disallowed. If $\Gamma_\gamma \ll \Gamma_{ppc}$ then $\Gamma_{\rm eff} \simeq \Gamma_\gamma$, and the expressions become identical. On the other hand, if $\Gamma_{ppc} \ll \Gamma_\gamma$ then $\Gamma_{\rm eff} \simeq \Gamma_{ppc}$, and photon emission dominates over the strong decay channel.

Independent of validity of the simplified rate expression in Eq. (24), the process can still be either direct or sequential, or for that matter any mixture. This is perhaps better appreciated by explicitly explaining that Γ_γ is determined entirely by the excited and ground state short-distance properties, while the strong decay is entirely determined by the structure underlying the barriers which has to be overcome before the reaction is completed. The effective thickness of the barrier is determined by the three-body resonance energy level.

The intermediate structure can be directly investigated by the density distribution of the corresponding angular wave function from Eq. (11). The angular wave function

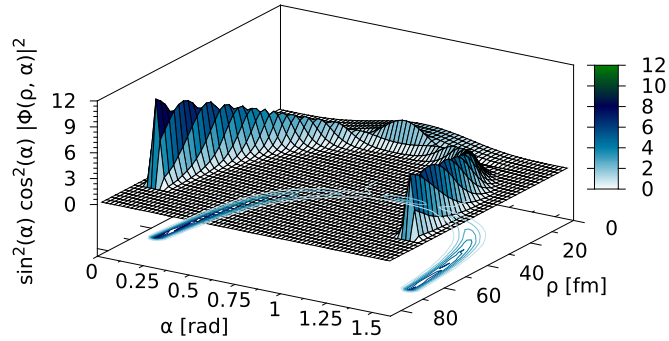

FIG. 8. The square of the angular wave function Φ from Eq. (12), multiplied by the phase factor $\cos^2(\alpha)\sin^2(\alpha)$ and integrated over Ω_x and Ω_y, as a function of ρ and α for the lowest λ of the 2^+ state in the second set of Jacobi coordinates.

corresponding to the lowest λ_n is shown in Fig. 8 as a function of ρ and α_{pc}. The structure is abundantly clear for ρ values larger than about 20 fm. The probability distribution is only finite at large and small α_{pc}, which through Eq. (4) implies that the distance is small between either the core and the first proton, or the second proton and the center of mass of the core-proton system. This is precisely the proton-core resonance configuration properly antisymmetrized. As this is the configuration for the lowest λ_n, the energetically most advantageous escape route is apparently through this configuration corresponding to sequential decay. However, this conclusion may change with relative sizes of the two- and three-body resonance energies, and as a function of the total three-body energy. The angular wave functions corresponding to higher-lying λ_n eigenvalues have different configurations. By including all the relevant, relatively low-lying λ spectrum, all the relevant angular configurations, and thereby all the relevant reaction mechanisms, are included, and not just the extreme sequential or direct paths.

The decay width from resonance to three particles can be estimated by use of the WKB tunneling probability through the lowest potential barrier. This is most accurately done using numerical integration between the classical turning points where the effective potential equals the three-body resonance energy, $V_{\rm eff}(\rho_0) = V_{\rm eff}(\rho_t) = E_R$. Based on the energy difference from the potential minima to the resonance energy, the harmonic oscillator frequency ω_0 can be determined. The knocking rate from Ref. [31] is about ω/π which must be multiplied by the second order WKB tunneling probability, $1/[1 + \exp(2S)]$, that is

$$\Gamma_{ppc} = \frac{\hbar\omega_0}{\pi}[1 + \exp(2S)]^{-1},$$
$$S = \frac{1}{\hbar}\int_{\rho_0}^{\rho_t} \sqrt{2\mu_{p,cp}[V_{\rm eff}(\rho) - E_R]}\, d\rho. \tag{30}$$

The Γ_γ width can be calculated using Eq. (22). The effective width $\Gamma_{\rm eff}$ can be calculated from Γ_γ and Γ_{ppc}. The values of these key quantities for the three-body decay, relating to the cases of practical interest studied in the previous sections, are presented in Table III. We find in almost all our Borromean cases that A^* is a well defined resonance with a very narrow

TABLE III. The three-body resonance energy along with both photon decay width calculated using Eq. (22) and proton decay width based on a WKB calcualtion. The effective width $\Gamma_{\rm eff}$ is calculated from these values. The cases of interest correspond to the peaks in Fig. 6. All energies and widths are in MeV.

State	E_R	Γ_{ppc}	Γ_γ	$\Gamma_{\rm eff}$
$2^+ : p_{3/2} + f_{5/2}$	1.14	4.1×10^{-9}	5.3×10^{-10}	4.7×10^{-10}
	2.17	5.9×10^{-3}	8.3×10^{-10}	8.3×10^{-10}
	4.29	3.0×10^{1}	2.7×10^{-8}	2.7×10^{-8}
$2^+ : p_{3/2}$	1.38	2.4×10^{-7}	5.4×10^{-10}	5.4×10^{-10}
	3.68	9.6×10^{-1}	1.5×10^{-8}	1.5×10^{-8}
$1^- : p_{3/2} + d_{5/2}$	0.61[a]		1.7×10^{-6}	
	1.50[b]	5.2×10^{-7}	1.0×10^{-5}	4.9×10^{-7}

[a] $E_{2b}(p_{3/2}) = E_{2b}(d_{5/2}) = 0.641$ MeV.
[b] $E_{2b}(p_{3/2}) = 0.641$ MeV, $E_{2b}(d_{5/2}) = 1.50$ MeV.

width. The reason is readily found in the potentials, where the attraction is sufficiently strong, inside very pronounced confining barriers, to hold a narrow resonance. As seen in Eq. (22) Γ_γ depends on the resonance energy, but it is dominated by the overlap matrix element for the given multipole transition. As such it increases slowly with energy irrespective of partial waves, but it changes dramatically when the order of the transition is changed. The increase is much more drastic for Γ_{ppc} as it depends exponentially on barrier thickness.

When the energy of the 1^- state is increased, by increasing the energy of the $d_{5/2}$ single-particle proton levels, the resonance becomes wider. The attractive pockets of the potentials diminish while moving to higher energies, implying that the resonance features disappear. The continuum states would then have substantially less relative probability at distances comparable to the size of the ground state. This decreases the rate of the $1^- \to 0^+$ transition. We emphasize that the method of the numerical calculations is completely unchanged, and the results are in fact obtained without any information about whether such a resonance exists or not.

For the lowest resonance the Γ_{ppc} is only about an order of magnitude larger than Γ_γ. This implies the lowest resonance is at the edge where the effective width becomes a mixture of the two. As Γ_{ppc} decreases exponentially with E_R without lower limit, while Γ_γ decreases as $E_\gamma^{2\ell+1}$, where the photon energy necessarily is finite, $\Gamma_{\rm eff}$ will be dominated by Γ_{ppc} if the resonance energy is lowered.

If the three-body resonances E_R are the only intermediate configurations acting as doorway states, then nonvanishing processes occur only when $E \approx E_R$ where the uncertainty is determined by the width of the states. On the other hand, small rates and cross sections arise also for energies without the match to resonance doorway states. The rate is calculated from the theoretical formulation for given energy, but the applications are rather for given temperature T. The temperature smearing over the energies up to around T then all contribute, and the higher energy contributions become exponentially suppressed. A much more detailed discussion can be found in Ref. [30].

The character of the reaction mechanism as sequential, direct, a mixture, or something else, is fundamentally determined by the dynamic evolution from small to large distances. However, a number of rather solid conjectures can be made from the calculated static properties. This can be elucidated with two schematic potentials based on extreme geometric progression corresponding to sequential and direct decay, for more details see Ref. [45]. Outside the strong attractive region the Coulomb potential for one proton moving away from the proton-core state of given positive energy E_{pc} is given by $V_{\rm seq} = (Z_c + 1)e^2/\rho + E_{pc}$. In case of several possible, different two-body energies the most likely potential to tunnel through would be the small and narrow potential. If the two protons are moving away from the core along the most favored symmetric linear configuration with the same ρ the potential is instead $V_{\rm dir} = (2Z_c + 1/2)e^2\sqrt{2}/\rho$, where $Z_c|e|$ is the core charge. These two potentials, $V_{\rm seq}$ and $V_{\rm dir}$, cross each other at ρ_c for an energy V_c, that is

$$\rho_c = \frac{e^2((2\sqrt{2}-1)Z_c - 1 + 1/\sqrt{2})}{E_{pc}} \approx \frac{2.6Z_c}{E_{pc}}, \quad (31)$$

$$V_c = E_{pc}\frac{(2Z_c + 1/2)\sqrt{2}}{(2\sqrt{2}-1)Z_c - 1 + 1/\sqrt{2}} \approx 1.6E_{pc} \quad (32)$$

for $Z_c \gg 1$. With $E_{pc} = 0.641$ MeV and $Z_c = 34$, we get $\rho_c = 139$ fm and $V_c = 1.00$ MeV, which is significantly further out than the potential thickness in Fig. 4(a). The most energetically favorable decay path is then the sequential path, barring drastic, and most likely energy demanding, changes in the configuration during the decay process. As $E_{3b} \simeq E_{2b}$ for 1^- the potential thickness is tending towards infinity, which would exclude a sequential decay.

The reaction mechanism for photodissociation, or equivalently radiative capture, of given energy E can then be expected characterized as sequential for $V_c < E$, mixed sequential direct for $E_{pc} < E < V_c$, mixed direct and virtual sequential $E < E_{pc} < V_c$, and direct $E \ll E_{pc}$ [44,46]. We emphasize that these characteristics are not rigorous properties, although limiting cases would be observable [47], as they would leave distinct signatures in the energy distribution of the emerging fragments. Based on these limits the reaction mechanism can very convincingly be classified as sequential for the 2^+ case, direct for the low-lying 1^- case, and either sequential or a mixture for the high-lying 1^- case. It should be noted that this is very strongly dependent on the specific potential depths and the temperature in question. For temperatures significantly higher or lower than the resonance energy the reaction mechanism would not be determined by the single lowest resonance, but by the continuum background contribution or possibly a complicated combination of several different resonances.

B. Energy level predictions

The central parameters in the effective lifetimes of the critical waiting points are the proton binding energies of the two following isotones. Ideally, one would like to predict these two- and three-body energies exactly. Unfortunately, insufficient experimental knowledge makes such predictions difficult. However, as seen in Sec. III A, it is possible to

establish relations between the possible two-body energies and the needed three-body energies. From there limits can be inferred regarding the position of low-lying excited energy levels in both the two- and three-body system.

As the critical waiting points are Borromean in nature the core-proton system must be unbound, while the two-proton system must be bound. In other words, the region of interest is limited to $E_{2b} > 0$ and $E_{3b} < 0$. The following limits are calculated without including a three-body potential. Adding an attractive three-body potential would lower the three-body energy, and thereby increase the estimated energy ranges.

If the ground state proton separation energy S_p is greater than 0.35 MeV (where the highest single wave curve in Fig. 2 crosses zero), then there must be a very close lying first excited core-proton state for the three-body system to be bound. Depending on the S_p value a very narrow energy range for this excited level can be predicted. Likewise, S_p cannot be greater than 0.74 MeV (where the $p_{3/2} + f_{5/2}$ curve crosses zero in Fig. 2), as the three-body system then could not be bound. Of course, this is based on the assumption that shell model predictions and the mirror nuclei correctly identifies the relevant single-particle states in the given region.

The only thing missing, if proper estimates are to be made concerning the waiting point nuclei, is the two-body energies. However, even this is not as severe a limitation as might be imagined. Based on the results in Fig. 2 energy intervals can be established for the proton separation energy. Recently, it was possible to measure the ground state proton separation energy of ^{69}Br to $S_p(^{69}\mathrm{Br}) = 641(42)$ keV [40]. For this to comply with our result the ground state must be either a $p_{3/2}$ or a $f_{5/2}$ state, with the other being a low-lying excited state, otherwise the three-body system would be unbound. In Ref. [40] the ground state is surmised to be a $f_{5/2}$ state with a $p_{3/2}$ state lying an unknown distance above. All lines allowing only one partial wave have crossed into the unbound three-body region before $E_{2b} = 0.641$ keV. The same is true for the $f_{5/2} + p_{1/2}$ line. The only remaining possibility among the likely partial waves is the $p_{3/2} + f_{5/2}$ combination.

The upper and lower limits for this first excited state can now be established from the relation between two- and three-body energy. The lower limit is of course $E_{2b}(p_{3/2}) = 0.641$ MeV, corresponding to a degenerate ground state. The upper limit is determined by keeping the $f_{5/2}$ energy constant and varying the $p_{3/2}$ energy. Setting $E_{2b}(f_{5/2}) = E_{2b}(p_{3/2}) = 0.641$ MeV results in $E_{3b} = -0.21$ MeV. By slowly changing $E_{2b}(p_{3/2})$ the upper limit is found to be at $E_{2b}(p_{3/2}) = 0.800$ MeV, where $E_{3b} = -0.00$ MeV. The first excited $p_{3/2}$ state in ^{69}Br is then predicted to lie less than 0.16 MeV above the ground state. Likewise, using the estimates included in the AME 2012 collection, a proton separation energy of $S_p(^{73}\mathrm{Rb}) = 0.6$ MeV is predicted [48]. This implies the ground and first excited states consist of a $p_{3/2}$ and $f_{5/2}$ state, one lying no more than 0.2 MeV from the other. For ^{65}As the AME estimated proton separation energy is at 0.09 MeV, which makes it difficult to predict anything specifically. However, it does make it very unlikely that there is a $p_{1/2}$ or a $f_{5/2}$ ground state without a low-lying first excited state.

Similar predictions can be made concerning the excited continuum levels. Based on Fig. 5 the 2^+ state is found to very consistently be 1.38 MeV above the ground state. The lower limit of the resonance energy E_R then corresponds to the lower limit of the ground state, i.e., $E_R^{\min} = 2 \times 0.641\,\mathrm{MeV} - 1.54\,\mathrm{MeV} + 1.38\,\mathrm{MeV} = 1.12\,\mathrm{MeV}$. Likewise, the upper limit corresponds to where the ground state is at the edge of being unbound, i.e., $E_{2b} = 0.74$ MeV and $E_R^{\max} = 1.38$ MeV. This very narrow interval can be used to estimate limits for the reaction rate.

It is considered much more unlikely that the three-body system will form a 1^- state based on both mean field calculations and comparisons with mirror nuclei. However, as has been shown, if it is even remotely possible the dipole transition will dominate the reaction rate. The placement of the 1^- resonance is not as sharply limited as the 2^+ resonance, which is dictated by the lowest two-body resonance. On the other hand, the 1^- resonance needs a combination of opposite parity states, and could move to arbitrarily high energies without affecting the 0^+ ground state.

C. Rate predictions

In the preceding sections it was argued that very narrow resonances will be produced by the fairly attractive short-distance region in combination with the wide Coulomb barrier at large distances. In addition, very confining limits have been placed on both two- and three-body energy levels. Collectively, this allows for limits to be placed on the relevant three-body reaction rates for specific energies. These limits would again be affected by the addition of a three-body potential. However, the energy scaling is predicted by Eqs. (19) and (24). More generally, this provides a method for estimating proton capture rates for the region in general given few experimental data.

As the reaction rate is dominated by narrow resonances it can well be approximated by Eq. (24) for temperatures in the 0.1–4-GK range. The limits of the resonance energy was established in Sec. V B for the specific case of the critical waiting points. Assuming the overlap matrix element is constant for small changes in two-body energy, Γ_γ only depends on photon energy as $E_\gamma^{2\ell+1}$. However, as the distance between the curves in Fig. 5 is constant, E_γ would also be constant independent of two-body energy. The same is therefore true of Γ_γ, and the Γ_γ value from Table III can be used for a given resonance. As $\Gamma_{\mathrm{eff}}^{-1} = \Gamma_{ppc}^{-1} + \Gamma_\gamma^{-1}$ the largest possible value of Γ_{eff} is the constant Γ_γ.

It is then clear that using Eq. (24) the largest rate is achieved at the lowest resonance energy where $\Gamma_{\mathrm{eff}} \simeq \Gamma_\gamma$. At some point, for sufficiently low resonance energies, the $\Gamma_{\mathrm{eff}} = \Gamma_\gamma$ assumption no longer holds as Γ_{ppc} continues to decrease. For lower resonance energies $\Gamma_{\mathrm{eff}} < \Gamma_\gamma$ and the rate decreases.

To estimate the rate it is then necessary to estimate Γ_{ppc} which means the barrier must be determined very accurately. Unfortunately, the intermediate distances that are relevant here are notoriously difficult to treat accurately by simple expressions. For large distances approximation such as the V_{dir} and V_{seq} potentials presented earlier could be used. These will however overestimate the potential, which will underestimate of the rate exponentially. A more appealing alternative is to use the potential calculated in full in Sec. IV A. The potential outside the barrier is the determining part. To study the rate

based on a two-body energy different from the value of 0.641 MeV this part of the potential needs to be shifted an amount corresponding to the difference in two-body energies.

The final procedure in estimating the three-body reaction rate is as follows. The first step is to assess the two-body energies somehow. For waiting point nuclei limits can be established from Fig. 2. The second step is to find the three-body energies based on the two-body energies. The ground state three-body energy is determined from Fig. 2, while the first excited level is determined from Fig. 5. If different two-body energies are used for the relevant partial waves the lower limit for the three-body energy is given by the curve where the energy is the same, while the upper limit is given by the highest single wave curve. The third step is to estimate $\Gamma_{\rm eff}$. The value of Γ_γ is given in Table III for the most likely cases. Otherwise the single-particle decay rates can be used to estimate Γ_γ [31], where a factor of 2 should be added to account for the two particles. In many cases $\Gamma_\gamma \ll \Gamma_{ppc}$, and the exact value of Γ_{ppc} is then not relevant. When necessary, for relatively low resonance energies, Γ_{ppc} can be estimated with a WKB calculation through the known potential barrier shifted appropriately according to the two-body energy. The fourth and final step is to calculate the limits of the reaction rate with Eq. (24) using the calculated effective width and the limits on the resonance energy. This method applies generally for proton capture in the region around the critical waiting points. If considering ^{64}Ge or ^{70}Kr instead of ^{68}Se minor changes in the long-range Coulomb potential would have to be considered, but the most important change would be the two- or three-body energy spectrum. The same method could be applied based on estimates of the particular energy levels.

The result is seen in Fig. 9, where the $2^+ \rightarrow 0^+$ rate is estimated based on three different two-body energies. The energy studied in Sec. IV A is used along with the upper energy level of $E_{2b} = 0.74$ MeV established in Sec. V B and an

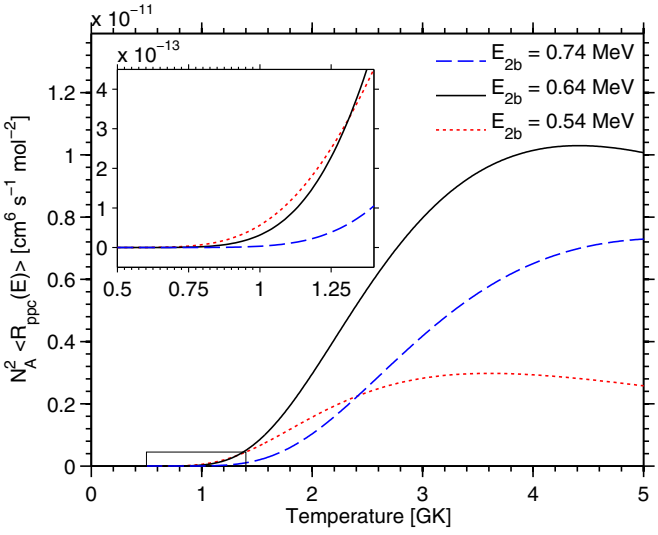

FIG. 9. Estimates of the reaction rate for $2^+ \rightarrow 0^+$ with $p_{3/2}$ and $f_{5/2}$ based only on two-body energies. The blue curve at $E_{2b} = 0.74$ MeV corresponds to the upper limit established in Sec. V B. The low temperature region has been scaled up to demonstrate the similarities.

energy an equal amount below. The low temperature region is scaled up to show how closely the rates agree for temperatures below ∼1 GK. The rate decreases with increasing resonance energy because of the exponential factor in Eq. (24), and it also decreases with decreasing resonance energy because we are at the edge where Γ_{ppc} starts affecting $\Gamma_{\rm eff}$. Changing the various two-body energies individually, between 0.54 and 0.74 MeV, would change the three-body resonance energy, but the final reaction rate would be within the limits here presented. Going outside this two-body energy region would decrease the rate exponentially, based on Eq. (24), for temperatures around 1–4 GK.

These limits are based on the assumption that only the lowest resonance contributes significantly. The temperature must be in the vicinity of the three-body energy for this to be true. For much lower temperatures the resonance energy is not accessible, and the main contribution is through off-resonant reactions. This would lower the rate exponentially. For higher temperatures other resonances would contribute, and the lowest resonance might only contribute through the tail of the cross section.

In principle, these rate estimates should include the various contributions discussed at the end of Sec. IV B, even for temperatures in the 1–4-GK region. However, these are all minor corrections which does not change the result significantly. Major changes would only occur with changes in energy levels.

VI. CONCLUSION

The waiting points in the *rp* process are prime candidates for three-body calculations by their very definition. Given the heavy core in the three-body system the proton-core interaction will determine the characteristic of the system, with only minor corrections stemming from the proton-proton interaction. Because of this, very simple relations between the two- and three-body energies can be derived and understood based on the three-body Hamiltonian. These relations apply equally well for both ground and excited energy levels. These very simple, and rather general, relations between two- and three-body structures and energies allow for the estimation of either two- or three-body properties given very sparse experimental data.

It is also seen that the three-body structure consists of the two protons located at the surface of the heavy core. At larger distances the structure is that of a single proton moving away from a two-body core-proton resonance. Conceptually, this corresponds to what is traditionally known as sequential decay. For low available initial three-body energy (and low temperature) this configuration would no longer be the energetically most favorable.

When calculating the cross section for the process $A + \gamma \rightarrow p + p + c$ the effective potential confining the particles is decisive. The relatively heavy core gives rise to a large Coulomb barrier and an attractive short-distance potential. This makes the lowest continuum states narrow, well-defined resonances. Based on the spectrum of the mirror nuclei, 2^+ states were assumed to dominate the low-lying spectrum. The full three-body rate calculation was based on the entire 2^+ spectrum. Assuming the narrow, well-defined resonances

have a Breit-Wigner shape, the full rate calculation could be reproduced from around 0.5 GK and up to 4 GK based solely on the lowest resonance. Summing over the contributions from the first few resonances for the 2^+ case increased this temperature range to about 5–6 GK. The off-resonance, background contribution is mainly relevant for lower temperatures, where the chance of accessing the resonance level is much smaller. For the much more unlikely 1^- case only one resonance state is present, which then dominates a wide temperature range around the resonance energy.

In the unlikely scenario where an 1^- state is available, depending on its position, the $\mathcal{E}1$ transition could contribute significantly. However, based on both mean field calculations and experimental measurements in the region around the critical waiting points single-particle orbitals of like parity dominate the low-lying energy levels. Also no 1^- state is seen in the mirror nuclei. This very effectively excludes three-body states of negative parity. The most likely transition is then the always allowed (as long as more than s waves are available) $\mathcal{E}2$ transition.

As the expression based on the assumed Breit-Wigner shape depends mainly on the resonance energies, the relations between two- and three-body energies can be used to provide limits for the reaction rate. Alternatively, the rate estimates could also be based directly on three-body resonance energies if available.

An added benefit of the three-body formalism is that no assumptions regarding the preferred reaction path are needed. On the contrary, the most likely reaction mechanism can be deduced based on the structure of the angular wave functions corresponding to the lowest λ_n eigenvalues. For most of the relevant energies the mechanism can be considered sequential through narrow two-body resonances. This is intuitively understandable if the three-body excited resonance state has a higher energy than the resonance(s) of the subsystem. On the other hand, a very low temperature only allows direct decay (or capture) since then the available energy is too low to populate the two-body resonances even virtually. However, these reaction questions would eventually have to be answered by studying the dynamic evolution from small to the large distances in more detail.

In conclusion, we have performed a full three-body analysis of the nuclear structure and decay of critical waiting points in the rp process. This allowed us to study in detail the two-proton capture rate needed to bridge the waiting points, as well as the energy levels central in determining the effective lifetimes of these waiting points in a stellar environment. We find that a simple expression, based on an assumed Breit-Wigner shape, can accurately reproduce the full three-body rate calculation in the temperature region 0.5–5 GK generally considered to be of astrophysical interest. This led to a general method for estimating two-proton capture rates in the region around the critical waiting points based only on either the two- or three-body energies, if these are more readily available. Specifically, we predict, given the currently available experimental data, that the two-proton capture rate forming ^{70}Kr for temperatures between 2 and 4 GK increase by a factor of 3.5 from $0.4 \times 10^{-11} N_A^2$ cm^6 s^{-1} mol^{-2}.

ACKNOWLEDGMENTS

The authors are grateful to K. Riisager for fruitful discussions and thoughtful insights. This work was funded by the Danish Council for Independent Research DFF Natural Science and the DFF Sapere Aude program, and partly supported by funds provided by DGI of MINECO(Spain) under Contract No. FIS2011-23565. We also acknowledge financial support from the European Research Council under ERC starting grant LOBENA, Grant No. 307447.

[1] R. K. Wallace and S. E. Woosley, Astrophys. J. Suppl. Ser. **45**, 389 (1981).
[2] H. Schatz, A. Aprahamian, J. Görres, M. Wiescher, T. Rauscher, J. F. Rembges, F.-K. Thielemann, B. Pfeiffer, P. Möller, K.-L. Kratz, H. Herndl, B. A. Brown, and H. Rebel, Phys. Rep. **294**, 167 (1998).
[3] G. Wallerstein *et al.*, Rev. Mod. Phys. **69**, 995 (1997).
[4] H. Schatz, A. Aprahamian, V. Barnard, L. Bildsten, A. Cumming, M. Ouellette, T. Rauscher, F. K. Thielemann, and M. Wiescher, Phys. Rev. Lett. **86**, 3471 (2001).
[5] I. J. Thompson and F. M. Nunes, *Nuclear Reactions for Astrophysics* (Cambridge University Press, Cambridge, UK, 2009).
[6] B. A. Brown, R. R. C. Clement, H. Schatz, A. Volya, and W. A. Richter, Phys. Rev. C **65**, 045802 (2002).
[7] J. Görres, M. Wiescher, and F.-K. Thielemann, Phys. Rev. C **51**, 392 (1995).
[8] H. Schatz, Int. J. Mass Spectrom. **251**, 293 (2006).
[9] O. Koike, M. Hashimoto, K. Arai, and S. Wanajo, Astron. Astrophys. **342**, 464 (1999).
[10] L. V. Grigorenko and M. V. Zhukov, Phys. Rev. C **72**, 015803 (2005).
[11] A. Wöhr *et al.*, Nucl. Phys. A **742**, 349 (2004).
[12] P. Schury, C. Bachelet, M. Block, G. Bollen, D. A. Davies, M. Facina, C. M. Folden, C. Guenaut, J. Huikari, E. Kwan, A. Kwiatkowski, D. J. Morrissey, R. Ringle, G. K. Pang, A. Prinke, J. Savory, H. Schatz, S. Schwarz, C. S. Sumithrarachchi, and T. Sun, Phys. Rev. C **75**, 055801 (2007).
[13] X. L. Tu, H. S. Xu, M. Wang, Y. H. Zhang, Y. A. Litvinov, Y. Sun, H. Schatz, X. H. Zhou, Y. J. Yuan, J. W. Xia, G. Audi, K. Blaum, C. M. Du, P. Geng, Z. G. Hu, W. X. Huang, S. L. Jin, L. X. Liu, Y. Liu, X. Ma, R. S. Mao, B. Mei, P. Shuai, Z. Y. Sun, H. Suzuki, S. W. Tang, J. S. Wang, S. T. Wang, G. Q. Xiao, X. Xu, T. Yamaguchi, Y. Yamaguchi, X. L. Yan, J. C. Yang, R. P. Ye, Y. D. Zang, H. W. Zhao, T. C. Zhao, X. Y. Zhang, and W. L. Zhan, Phys. Rev. Lett. **106**, 112501 (2011).
[14] A. S. Jensen *et al.*, Rev. Mod. Phys. **76**, 215 (2004).
[15] M. V. Zhukov *et al.*, Phys. Rep. **231**, 151 (1993).
[16] P. G. Hansen and B. Jonson, Europhys. Lett. **4**, 409 (1987).

[17] A. Bartlett, J. Gorres, G. J. Mathews, K. Otsuki, M. Wiescher, D. Frekers, A. Mengoni, and J. Tostevin, Phys. Rev. C **74**, 015802 (2006).
[18] D. Hove, D. V. Fedorov, H. O. U. Fynbo, A. S. Jensen, K. Riisager, N. T. Zinner, and E. Garrido, Phys. Rev. C **90**, 064311 (2014).
[19] V. D. Efros *et al.*, Z. Phys. A **355**, 101 (1996).
[20] D. V. Fedorov *et al.*, J. Phys. G **37**, 115105 (2010).
[21] R. de Diego *et al.*, Europhys. Lett. **90**, 52001 (2010).
[22] J. Giovinazzo, B. Blank, M. Chartier, S. Czajkowski, A. Fleury, M. J. Lopez Jimenez, M. S. Pravikoff, J.-C. Thomas, F. de Oliveira Santos, M. Lewitowicz, V. Maslov, M. Stanoiu, R. Grzywacz, M. Pfützner, C. Borcea, and B. A. Brown, Phys. Rev. Lett. **89**, 102501 (2002).
[23] E. Garrido, D. V. Fedorov, and A. S. Jensen, Nucl. Phys. A **733**, 85 (2004).
[24] J. Erler *et al.*, Nature (London) **486**, 509 (2012).
[25] W. E. Ormand, Phys. Rev. C **55**, 2407 (1997).
[26] M. Thoennessen, Rep. Prog. Phys. **67**, 1187 (2004).
[27] E. Nielsen *et al.*, Phys. Rep. **347**, 373 (2001).
[28] E. Garrido, D. V. Fedorov, and A. S. Jensen, Phys. Rev. C **69**, 024002 (2004).
[29] R. de Diego *et al.*, Phys. Lett. B **695**, 324 (2011).
[30] E. Garrido *et al.*, Eur. Phys. J. A **47**, 102 (2011).
[31] P. J. Siemens and A. S. Jensen, *Elements of Nuclei: Many-body Physics with the Strong Interaction* (Adison-Wesley, New York, 1987).
[32] A. J. Nicholas *et al.*, Phys. Lett. B **733**, 52 (2014).
[33] C. D. Nesaraja, Nucl. Data Sheets **115**, 1 (2014).
[34] J. K. Tuli, Nucl. Data Sheets **103**, 389 (2004).
[35] B. Singh, Nucl. Data Sheets **108**, 197 (2007).
[36] E. A. Mccutchan, Nucl. Data Sheets **113**, 1735 (2012).
[37] D. Abriola and A. A. Sonzogni, Nucl. Data Sheets **111**, 1 (2010).
[38] M. Oinonen, J. Äystö, A. Jokinen, P. Baumann, F. Didierjean, A. Huck, A. Knipper, M. Ramdhane, G. Walter, M. Huyse, P. Van Duppen, G. Marguier, Y. Novikov, A. Popov, D. M. Seliverstov, and H. Schatz (ISOLDE Collaboration), Phys. Rev. C **61**, 035801 (2000).
[39] E. Garrido, A. S. Jensen, and D. V. Fedorov, Phys. Rev. C **91**, 054003 (2015).
[40] Del Santo *et al.*, Phys. Lett. B **738**, 453 (2014).
[41] E. Garrido, Few-Body Syst. **56**, 829 (2015).
[42] W. A. Fowler, G. R. Caughlan, and B. A. Zimmerman, Annu. Rev. Astron. Astrophys. **5**, 525 (1967).
[43] L. V. Grigorenko, R. C. Johnson, I. G. Mukha, I. J. Thompson, and M. V. Zhukov, Phys. Rev. C **64**, 054002 (2001).
[44] R. Álvarez-Rodríguez, H. O. U. Fynbo, A. S. Jensen, and E. Garrido, Phys. Rev. Lett. **100**, 192501 (2008).
[45] E. Garrido *et al.*, Nucl. Phys. A **748**, 27 (2005).
[46] A. S. Jensen, D. V. Fedorov, and E. Garrido, J. Phys. G **37**, 064027 (2010).
[47] S. Chekanov *et al.*, Eur. Phys. J. C **51**, 289 (2007).
[48] G. Audi *et al.*, Chin. Phys. C **36**, 1287 (2012).